Wavelet analysis of the Voyager data on planetary rings. I. Description of the method

Ph. Bendjoya
Observatoire de Nice, B.P. 229, 06304, Nice cedex 04, France
e-mail: benchoc@franck.obs-nice.fr

J.-M. Petit
C.N.R.S.
Observatoire de Nice, B.P. 229, 06304, Nice cedex 04, France
e-mail: petit@bach.obs-nice.fr

F. Spahn
Working group "Nonlinear Dynamics" (MPG)
University Potsdam; D-O-1571 Potsdam; Germany
e-mail: spa@babel.aip.de

Abstract

In this paper we present a new method which allows us to extract signal from low (of the order of 1) signal to noise ratio data. The noise is almost completely removed, and the significance of the resulting signal is quantified against pure chance fluctuations. The technique is based on a wavelet transform, and uses a crude pattern–recognition algorithm in the space–scale plane to extract the interesting information. This method has been applied to simulated signals with signal to noise ratio ranging from 0.4 to 2. and the reconstructed signals are shown. From the wavelet transform coefficients, it is possible to gain some quantitative information on the size of the detected structures. As a first real case application, we present the analysis of the Encke gap ringlet in the Saturn's rings. We show that its detailed shape contain at least two peaks, and that its total width is about 8 km, while the width of the left peak is about 1.5 km.

1 Introduction

The Voyager 2 PPS data, obtained from the occultation of the star δ *Scorpii* by the Saturn's rings, have provided a spatial resolution in the radial direction better than 100 m (Lane *et al.* 1982 ; Esposito *et al.* 1983a). Many kinds of structures, at every scale length, have been discovered from these data in Saturn's rings. A certain number of papers have been devoted to the analyses of these data pointing out different kind of features such as density waves (Esposito *et al.* 1983a, 1983b; Brophy and Rosen, 1992), gaps (Petit and Hénon, 1988), sharp edges (Borderies *et al.* 1989),and wakes (Showalter *et al.* 1986). A global catalog of 216 features has been established by Esposito *et al.* 1987. The main philosophy of this catalog was to present the significant features, not to study the detailed shape of low signal-to-noise ratio features. It appears interesting to study such fine details in order to compare the observations with some theoretical models. Indeed, in what concerns a ringlet due to the presence of an embedded moonlet, different models lead to different shapes of the ringlet. This shape is strongly related to the orbital elements of the moonlet and its mass and size (Spahn *et al.* 1992). Another interest is to study structures like small variations in the optical depth as an indirect detection of large particles (from 100 m to a few kilometers in size) that are too small to be directly detected.

The purpose of this paper is to present a new method of signal processing based on the wavelet transform. This method allows us to detect, count and reconstruct localized bumps and/or depletions, with a drastic decrease of noise. Since this method is essentially a local one, the main limitation of this method occurs when one is trying to detect weak structures close to strong ones. An iterative process of analysis is then needed. The method is not based on any modelling of the noise (Gaussian, Poissonian ...), and gives, as it will be shown, satisfying results even for very low signal-to-noise ratio signals (of order of 0.5). In section 2 we briefly recall the principles of the wavelet transform and present the strategy we have applied to use this transform in detection of significant structures. In section 3 we applied this method on simulated signals. We show the details of the algorithm concerning : the noise elimination, the quantification of the significance of detected structures, and the behavior of the reconstructed signal as function of the level of significance. As a first real case application we present the reconstruction of the Encke gap ringlet.

2 The method

This section is divided in two parts. The first part gives a summary of the main results on the wavelet transform that will be used in this paper. More details can be found in Daubechies, 1988, Mallat, 1989 and Meyer, 1989. The second part describes the method we have built to extract information and remove noise from the wavelet transform coefficients.

2.1 Wavelets transform

We want to study a non–periodic signal $S(x)$ and obtain information on both the location and the size of the characteristic features (later on called structures). We first recall a few basics about the well–known Fourier transform.

The Fourier transform is good at giving the "frequency" (size). And it is a projection on an orthogonal basis. Hence, there exists a unique decomposition and reconstruction formula for a given function. But there is no relationship between the local behavior of $S(x)$ and the amplitude of the Fourier coefficients. This information is so deeply buried in the phases of the coefficients that it is not useful. Another problem is that the functions $\sin(x)$ and $\cos(x)$ are not compactly supported (they are not identically null outside of a finite interval). Therefore we need to know the behavior of $S(x)$ at infinity in order to compute the coefficients, unless we are dealing with a periodic signal. The Fourier coefficients are simply the inner products of $S(x)$ and a set of functions derived from two functions $\sin(x)$ and $\cos(x)$ by a scaling:

$$\sin(x) \rightarrow \sin(\omega x), \qquad \cos(x) \rightarrow \cos(\omega x) \tag{1}$$

The wavelet transform of $S(x)$ is the decomposition on a basis of functions $w_{a,b}(x)$, all derived from a unique function $w(x)$, called the "mother wavelet", by translation and scaling:

$$w_{a,b}(x) = a^{-1/2} w(a^{-1}(x-b)) \tag{2}$$

The coefficient $a^{-1/2}$ is not mandatory. One can choose any other exponent for a, depending on the kind of normalization one is interested in. The exponent $1/2$ is useful for normalizing the energy (the square of the modulus of the coefficients). The function $w(x)$ must satisfy a "compatibility condition":

$$\int_0^\infty \frac{|\hat{w}(\omega)|^2}{|\omega|} d\omega < \infty, \tag{3}$$

where $\hat{w}(\omega)$ is the Fourier transform of $w(x)$, in order to be a wavelet. This means, in particular, that the integral of the wavelet should vanish. It must also be well localized both in space and in scale. Mathematically speaking, we choose an integer r (r is called the order of the wavelet), and we impose the properties:

- For all $x \in R$ (set of reals), all $m \in N$ (set of natural integers), and $0 \le q \le r$, there exist C_m such that:

$$\left| \frac{d^q w(x)}{dx^q} \right| \le C_m (1 + |x|)^{-m}. \tag{4}$$

- The collection

$$2^{j/2}w(2^j x - k), \quad j \in Z, \quad k \in Z \tag{5}$$

is an orthonormal basis of $\mathcal{L}^2(R)$.

The first of these conditions insures the smoothness of $w(x)$, and both conditions together imply that the moments of $w(x)$, up to order r vanish. S. Mallat (1989) discovered a systematic approach to find solutions to this problem. I. Daubechies (1988) showed that, for any r, there exist compactly supported functions $w(x)$ satisfying the above conditions.

The wavelet coefficients of $S(x)$ are simply:

$$d_{j,k} = \int_{-\infty}^{\infty} S(x) w_{j,k}(x) dx, \tag{6}$$

and the unique way of recovering $S(x)$ from the coefficients is:

$$S(x) = \sum_j \sum_k d_{j,k} w_{j,k}(x). \tag{7}$$

The previous formula gives $S(x)$ as a sum of details from the finest scale to the largest one. One can also choose another orthonormal basis consisting of the collection $w_{j,k}(x)$, $j \in N$, $k \in Z$ (set of relative integers), together with the collection $q(x-k)$, $k \in Z$, where $q(x)$ is a new smooth function with a rapid decay at infinity. Obviously, the two functions $q(x)$ and $w(x)$ cannot be chosen independently. In this basis, $S(x)$ can uniquely be written as:

$$S(x) = \sum_{k \in Z} c_k q(x-k) + \sum_{j \in N} \sum_{k \in Z} d_{j,k} w_{j,k}(x) = E_0(S) + \sum_{j \in N} D_j(S) \tag{8}$$

where $c_k = \int_{-\infty}^{\infty} S(x) q_k(x) dx = \int_{-\infty}^{\infty} S(x) q(x-k) dx$. This means that $S(x)$ is the sum of a smooth part $E_0(S)$ and a sequence of finer and finer fluctuations $D_j(S)$. The function $q(x)$ is a smoothing function that allows us to cut the doubly infinite sum of eq. (7). The $q(x-k)$'s account for the large scale fluctuations, the $w_{j,k}$'s for the small ones. Obviously, the resolution corresponding to the smooth part can be chosen arbitrarily.

Consider now a real sampled signal. The ranges of variation of j and k are now finite. The scale range is defined by the sampling step for the smallest one (finest resolution) and the length of the signal for the largest (coarsest resolution). The range of variation of k is also defined by the length of the signal. Among the many possibilities for the two functions $q(x)$ and $w(x)$, we choose:

$$\begin{aligned} q(x) &= 1 - |x| \quad \text{for} \quad |x| \leq 1, \\ &= 0 \quad \text{otherwise}, \end{aligned} \tag{9}$$

and:

$$w(x) = \frac{|x|}{4} - \frac{1}{2} \quad \text{for} \quad 1 < |x| \leq 2,$$
$$= \frac{1}{2} - \frac{3|x|}{4} \quad \text{for} \quad |x| \leq 1, \tag{10}$$
$$= 0 \quad \text{otherwise,}$$

The process of computing the wavelet coefficients can be done iteratively. The first trivial step is to take the function $q(x)$ with the same resolution as the sampled signal. We only have to compute the c_k^0's (the superscript refers to the number of the step in the iterative process). From the formula for $q(x)$, one can see that the c_k^0's are simply the sampled values of $S(x)$ (the integrals are changed into summations since we are dealing with a discrete set of points). Then we consider a resolution twice as large. We choose the normalizing coefficients such that we replace $q(x)$ by $q(x/2)/2$. There is only one level of fine fluctuations to add to the smoothed part to recover the signal, and it is defined by the set of $d_{1,k} = d_k^1$. We can now repeat the same procedure to the smoothed part of level 1. This will give us two new sets of coefficients c_k^2 and d_k^2. With our choice of $q(x)$ and $w(x)$, the formulae to obtain the c_k^j's and the d_k^j's are very simple:

$$c_k^j = \frac{1}{2} c_k^{j-1} + \frac{1}{4} \left(c_{k-2^{j-1}}^{j-1} + c_{k+2^{j-1}}^{j-1} \right), \quad j \geq 1, \tag{11}$$

and:

$$d_k^j = c_k^{j-1} - c_k^j. \tag{12}$$

One can see that the c_k^j's are obtained by applying a low–pass filter to the c_k^{j-1}'s. The d_k^j's being obtained by a difference between two levels of c_k^j's are in fact the result of a band–pass filter applied to the signal. Due to the shape of the function $q(x)$, the associated wavelet $w(x)$ is often called the "linear wavelet".

For the reconstruction formula, things are quite simple. We are interested in reconstructing the sampled values, not the signal $S(x)$. When adding the c_k^j's and the d_k^j's, we get the c_k^{j-1}. Hence, the reconstruction formula is:

$$S(x_k) = c_k^{j_{max}} + \sum_{j=1}^{j_{max}} d_k^j, \tag{13}$$

where j_{max} is the maximum scale corresponding to the length of the signal.

A more general description of this method has been given by S. Mallat (1989) in the framework of the multiresolution analysis.

The wavelet transform described above is the one that allows us to work with the coefficients in order to remove the noise in a real signal (we are working with coefficients in an orthogonal basis).

2.2 Signal processing

Our aim is to use the wavelet transform as a signal processing tool to extract the behavior of the signal while removing the noise. We also want to have the possibility to compute the statistical significance of detections. The main philosophy of the procedure consists in isolating, in the space–scale plane where the wavelet transform of the signal is unfolded, the patterns made by coefficients pointing out structures with a level of significance versus the noise fluctuations. Then the signal is reconstructed from the selected coefficients. The patterns of significant wavelet coefficients are exhibited by means of a double thresholding. A first one is very restrictive, leading to the detection of very significant structures within the signal, with a drastic decrease of the noise, and a second one which allows the addition of more and more local details as it is chosen more and more permissive. These thresholdings are made scale by scale by comparing the wavelet coefficients derived from the studied signal to the distribution of coefficients computed from a pseudo–random signal. The pseudo–random signal is generated from the signal. For each point x_k of the signal, we draw at random a value $S_{pse}(x_k)$ of the pseudo–random signal, according to the probability distribution computed from the real signal. This strategy has already been applied in asteroid family detection (Bendjoya *et al.* , 1991) and allows us to take into account the intrinsic distribution of the noise instead of having to model it.

The wavelet transform of a white noise signal gives fluctuating coefficients, with no noticeable pattern in the space–scale plane (see Fig. 1). Also of importance is the fact that almost no coefficients deviate greatly from the mean. Fig. 1b displays a representation by a gray scale coding of the wavelet transform coefficients of the signal performed by means of the linear wavelet. The y-axis stands for the scales and the x-axis for the positions. For a given scale the value of a coefficient is coded by a gray level which varies linearly from black to white with the value of the coefficient in the range the mean of the coefficients plus or minus four times the standard deviation of the coefficients at the given scale. The normalization is made scale by scale. For a noiseless signal, there is a definite pattern in the space–scale plane (see Fig. 2). Particularly, some coefficients deviate by a large amount from the mean, and they tend to the mean on each side of the maximum for each scale (this is due to the absence of structures on each side), with a width proportional to the scale. In the following, in order to determine the mean and quantify a "large deviation", we evaluate the mean and standard deviation, for each scale, of the coefficients of the wavelet transform of a pseudo–signal $S_{ps}(x)$. As mentioned above, this pseudo–signal is a random data set having the same cumulative distribution as the

Fig. 1a

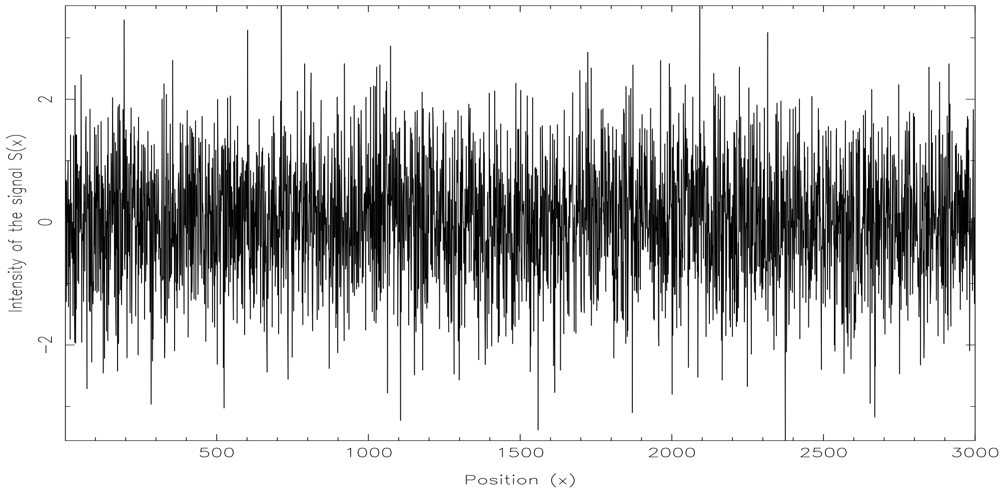

Fig. 1b

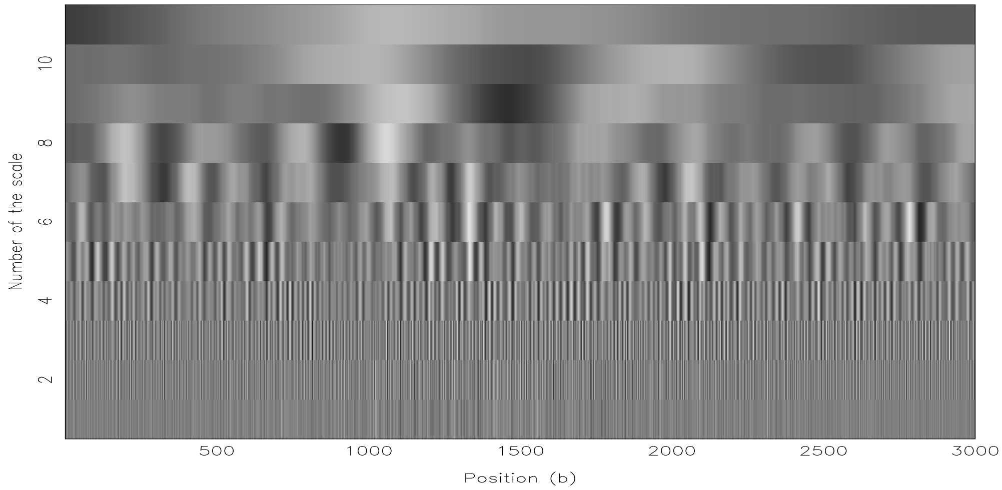

Fig. 1: a) A white noise signal. The x–axis is the position, and the y–axis is the signal intensity $S(x)$ b) Gray scale representation of the coefficients of the wavelet transform of the noise signal of Fig. 1a, using the linear wavelet (see section 2). The x–axis is the position, and the y–axis is the number of the scale. For a given scale the value of a coefficient is coded by a gray level which varies linearly from black to white with the value of the coefficient in the range the mean of the coefficients plus or minus four times the standard deviation of the coefficients at the given scale. The correspondence between value and gray level is made scale by scale.

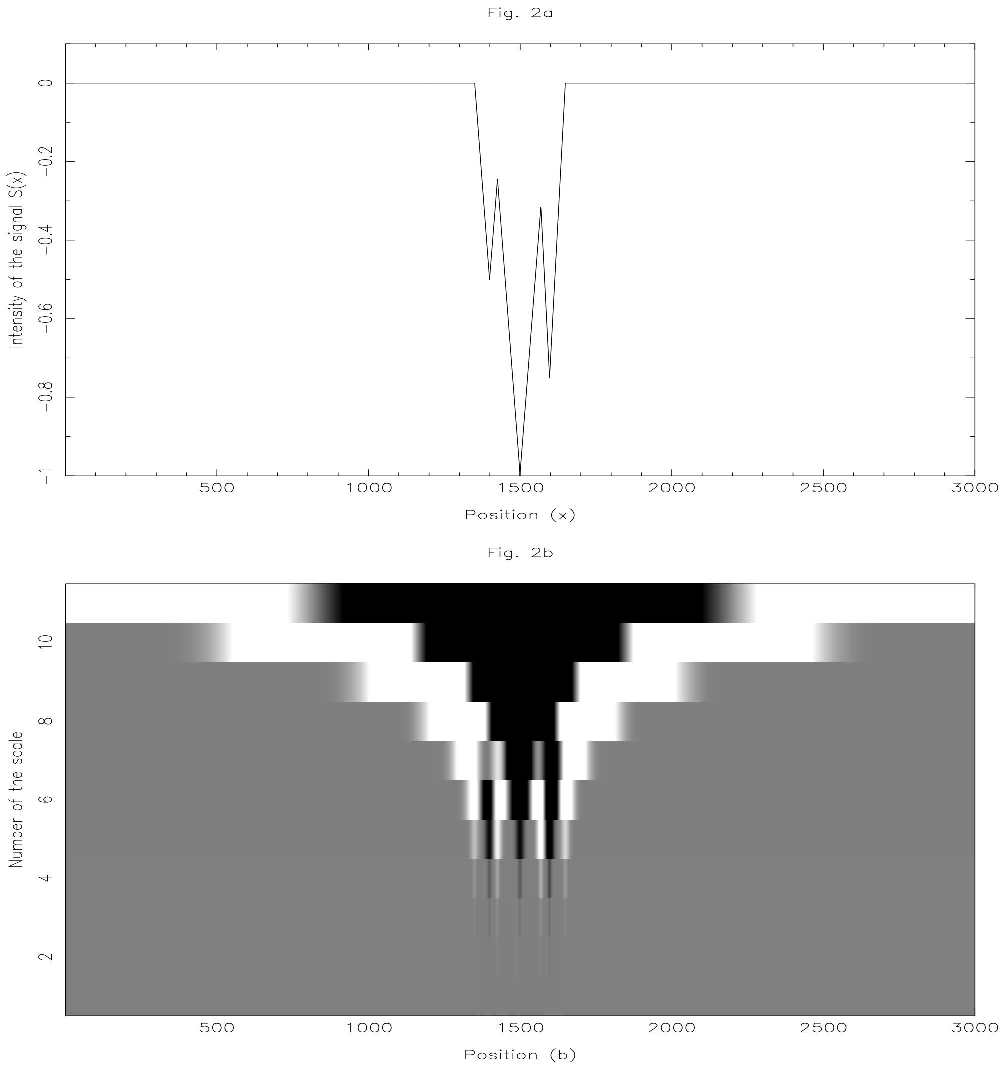

Fig. 2: a) A three peak noiseless signal artificially generated. b)Same as Fig. 1b for the signal of Fig. 2a.

signal under study $S(x)$.

We use a pattern–recognition algorithm in order to isolate the significant patterns in the space–scale plane. This is done by a double thresholding. First, we search for points in the space–scale plane with a very high level of significance (the seeds). Those seeds are the points where the coefficients deviate by a large amount, i.e. by more than a given number times the standard deviation, from the mean. This defines a first threshold, the seed–threshold $T_{se}(a_i)$. Usually we take $T_{se}(a_i) = 5\sigma_{S_{ps}}(a_i)$, where $\sigma_{S_{ps}}(a_i)$ is the standard deviation of the coefficients of scale a_i of the pseudo–random signal. The thresholding is done by retaining the points where the coefficients minus the mean, defined above, are larger (resp. smaller) than T_{se} (resp. $-T_{se}$) for a bump (resp. hole) detection. The seeds give a rough estimate of the size, position and shape of significant structures in $S(x)$. In order to add details to these detected structures, we need to take into account some coefficients in the vicinity of the seeds.

We define a second threshold, the skeleton–threshold T_{sk} which determines the points that might be associated with the seeds. Usually $1.5\sigma_{S_{ps}}(a_i) \leq T_{sk}(a_i) \leq 2\sigma_{S_{ps}}(a_i)$. Among the points that are selected by this second weaker threshold, those that are connected by nearest neighbor relation to a seed actually belong to a pattern. In other words, a wavelet coefficient is included if the absolute value of its difference from the mean value is above the threshold, and if it is adjacent to a "seed" either in the location index or the scale index direction. These new points are new seeds. The procedure of extension is iterated until no new point is added. As seen before (Fig. 2) a structure in $S(x)$ gives significant coefficients on a range of scales. The most significant ones, corresponding to the seeds which belong to restricted range of scales (see Fig. 5a). Therefore we have to extent the seed along the scale axis. Furthermore, at a given scale, only the coefficients in the middle of the structure are selected by the seed–threshold. However the structure contributes to coefficients that are not selected by T_{se} but are significant according to T_{sk} (see Fig. 5b). Then we must consider them. At this stage of the procedure we have a set of coefficients, with a level of significance defined by T_{sk} but the cores of the patterns thus defined are significant at the level defined by T_{se}.

Once we have determined the skeletons, we use the reconstruction formulae with the coefficients of the skeletons unchanged, and the other ones put scale by scale to the mean. Unfortunately, if we do so, the reconstruction of a bump (resp. hole) gives rise to a hole (resp. bump) on each side of the signal. Due to the shape of the analysing wavelet, a bump, for example, gives coefficients that are larger than the mean in its central part and smaller than the mean on its edges (see Fig. 3, the wavelet coefficients of a Dirac). Therefore, in order to avoid this reconstruction bias, we must include also the coefficients that are smaller than the mean in the vicinity of the skeleton of the bump. The size of the vicinity is the extent of the wavelet at each scale. A precise description of the algorithm to avoid the bias is done in Appendix A.

The different steps of the procedure can be summarized as follow : (i) a first restrictive thresholding T_{se} allows to localize the strongly significant structures within the signal, and eliminate nearly all noise; (ii) the seeds formed by the coefficients selected by T_{se} are then enriched along both the scale and the space axis by related coefficients coming from a second more permissive thresholding T_{sk}; (iii) in order to avoid some bias of reconstruction, some coefficients are considered in the vicinity of the skeletons defined by the enriched seeds; (iv) the non selected coefficients are changed to the mean of each scale; (v) the signal is reconstructed from the coefficients obtained after step (iv).

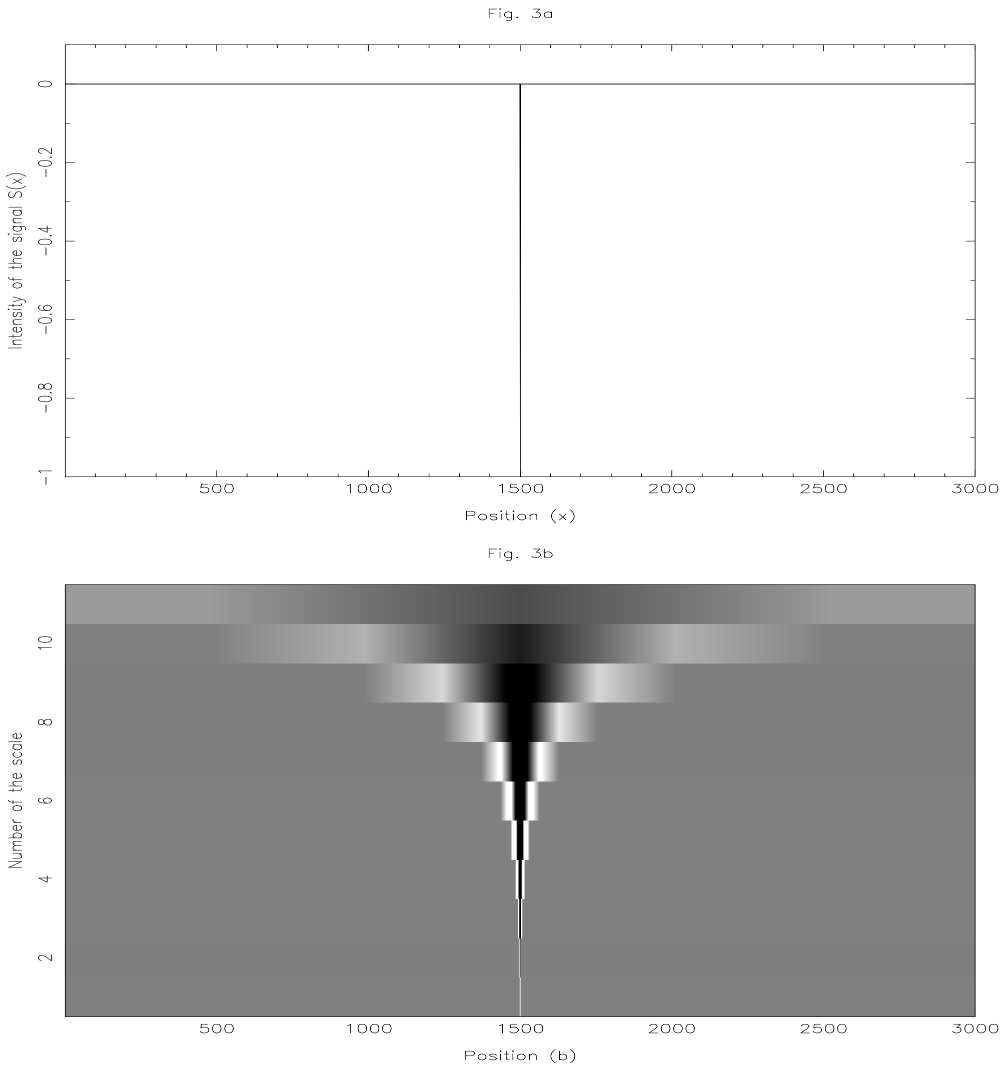

Fig. 3: a) A Dirac signal. b) Same as Fig. 1b for the signal of Fig. 3a.

3 Applications

3.1 Simulated signal

The models of gravitational interactions between the particles of a planetary ring and a moonlet orbiting within this ring has led Petit and Henon (1988) to exhibit the formation of a stable ringlet from numerical simulations. Collisions between particles were taken into account. This restricted the number of particles used in the simulations, which in turn prevented the analysis of fine details within the ringlet. The hydrodynamic approach of Spahn *et al.* (1992) allows us to propose as a stable solution a ringlet the density of which is inhomogeneous and presents a symmetric feature composed by three "peaks" in the distribution of matter.

By analyzing the Voyager data in the Encke gap of Saturn's A ring, Showalter (1991) detected the moonlet Pan which may be responsible for a ringlet in this area. The diameter of this moonlet was estimated by Showalter to be around 20 km. An analysis made by Spahn on the Voyager 2/PPS data by means of a *t-test* method seemed to show the presence of a three-peak structure (private communication). Unfortunately the very low signal to noise ratio (of order of 1) of the data prevented him from convingcingly detecting this peculiar structure with the methods he used. This signal exhibits different structures on a very large range of characteristic sizes. Therefore the wavelet transform appears well-suited for processing such a signal.

The idea is to create first a signal with a three–peaked structure and add to it different realizations of gaussian noise in order to simulate the Voyager data. The wavelet analysis method has been performed for different shapes of the three–peak structure, different signal to noise ratios and different realizations of the noise.

3.2 Wavelet coefficients

Fig. 2a shows a noiseless simulated three-peak structure and Fig. 4a the same with an added noise realization. We define the signal to noise ratio (S/N) as the ratio between the amplitude of the structure (here, 1) and the standard deviation of the gaussian noise we have added. This definition gives a local meaning to S/N. In our case, we are not interested in large scale structures but rather in local ones. Fig. 4a shows a signal to noise ratio of 1.2, since the standard deviation is 0.833 and the amplitude of the noiseless signal is 1.

Fig. 4b displays the gray level coded coefficients obtained from the wavelets analysis of the signal of Fig. 4a. Fig. 5a shows the coefficients selected by the first thresholding T_{se} (here, $T_{se}(a_i) = 5\sigma_{S_{ps}}(a_i)$). One can easily distinguish the patterns forming the seeds in the space–scale plane of the wavelet coefficients. One can also remark how the noise corresponding to the small scales is eliminated.

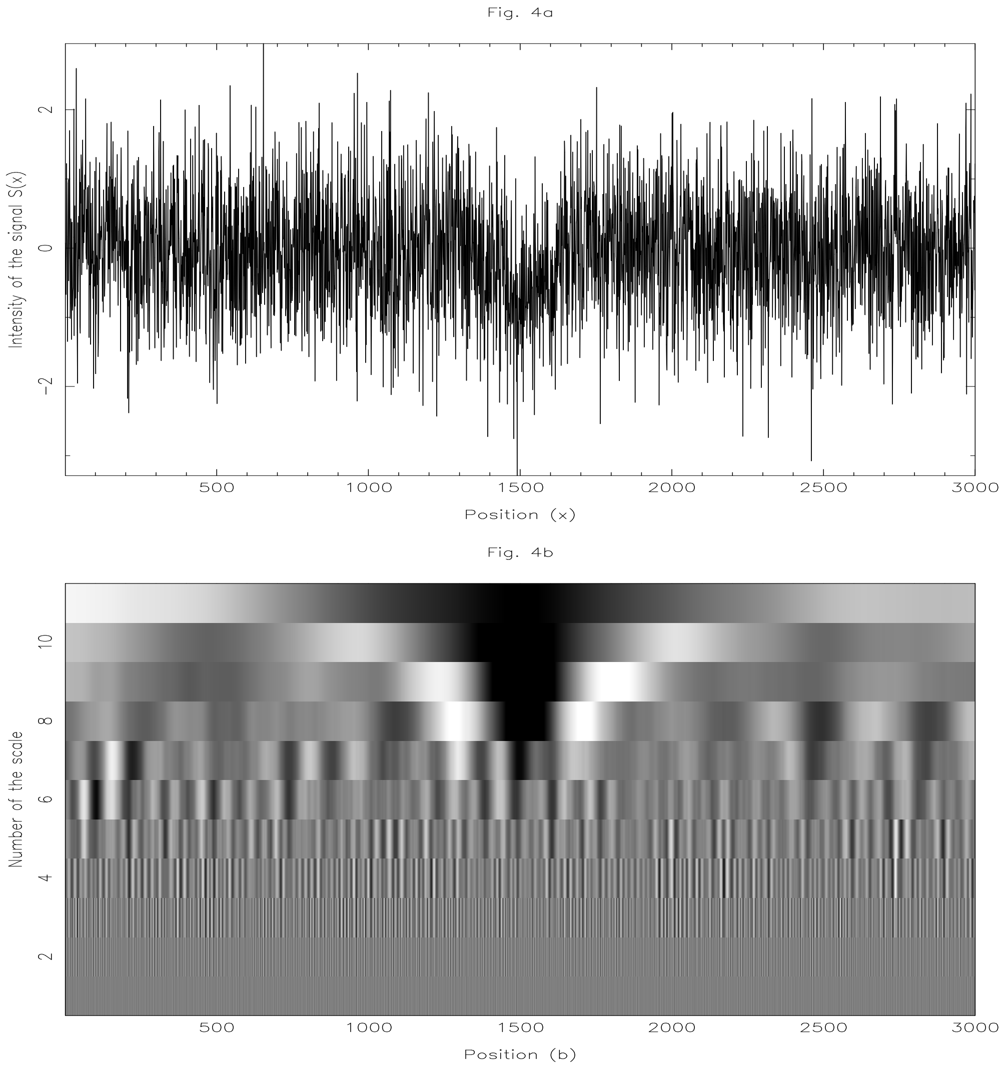

Fig. 4: a) Superposition of Fig. 2a and a white noise leading to a signal to noise ratio of 1.2. b)Same as Fig. 1b for the signal of Fig. 4a.

Fig. 5b shows the skeletons of coefficients created by adding to the seeds the connected coefficients coming from the second thresholding ($T_{sk}(a_i) = 1.6\sigma_{S_{ps}}(a_i)$) and also a contour plot of the coefficients added to avoid bias reconstruction (see section 2.2 step (iii)).

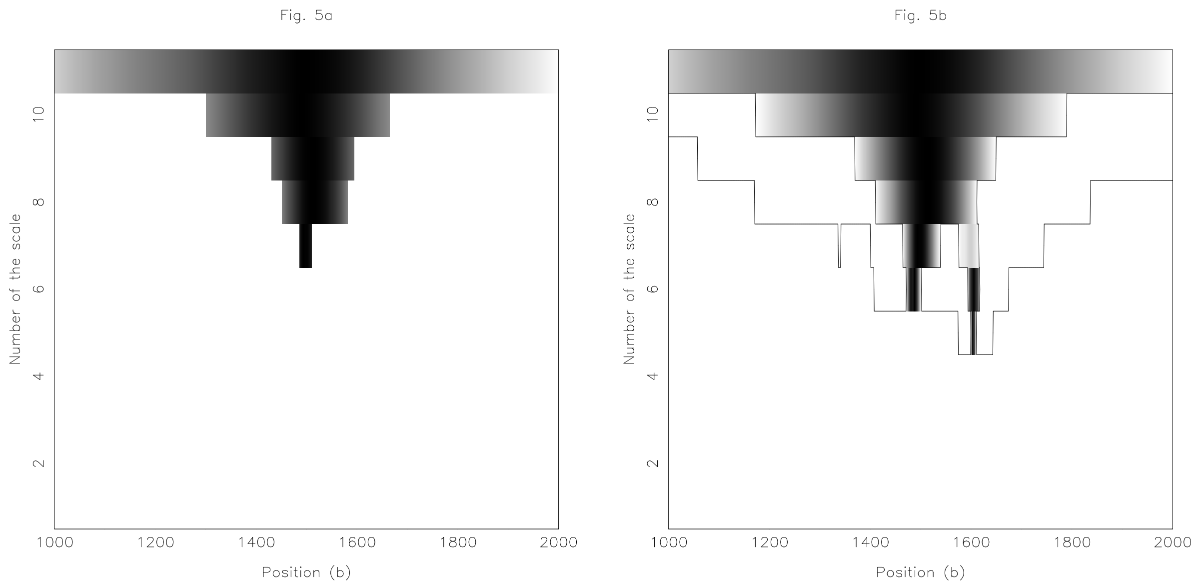

Fig. 5: a) Gray scale representation of the coefficients selected by the first and most restrictive thresholding ($T_{se}(a_i) = 5.0\sigma_{S_{ps}}(a_i)$), extracted from the coefficients of Fig. 4b (a zoom is made around the region of interest). b) Coefficients satisfying the second thresholding ($T_{sk}(a_i) = 1.6\sigma_{S_{ps}}(a_i)$) and connected to the previous ones have been added. The contour plot shows the location of positive coefficients added to avoid reconstruction biases.

3.3 Reconstructed signals

The main problem at this step of the analysis is to define the "best" second threshold. The "best" T_{sk} (quoted hereafter T^*_{sk}) must be understood as the threshold which is permissive enough to add fine details to the localized structures, but also strict enough to avoid the reappearance of localized sharp features, with a relatively large amplitude, and which can be associated with noise. One must keep in mind that there are always finite probabilities that some true features of the signal will be lost by thresholding and some noise spikes will make it through the threshold. The goal is to optimize the trade–off by picking the "best" threshold, avoiding any qualitative criterion. For the choice of T^*_{sk} we have developed a strategy relying on the philosophy of the wavelet transform.

The idea is to get an indicator of the presence of noise in the reconstructed signal and to choose T^*_{sk} as the value of the threshold for which this indicator changes suddenly. As we have already pointed out, the wavelet transform provides a multi-resolution analysis in which small details in the signal are represented at the small scales. More precisely the noise is mainly detected by the first scale. Therefore we compute the first scale of the wavelet transform on the reconstructed signals obtained for different T_{sk}. The indicator of the presence of noise is the standard deviation of the wavelet coefficients at this smallest scale.

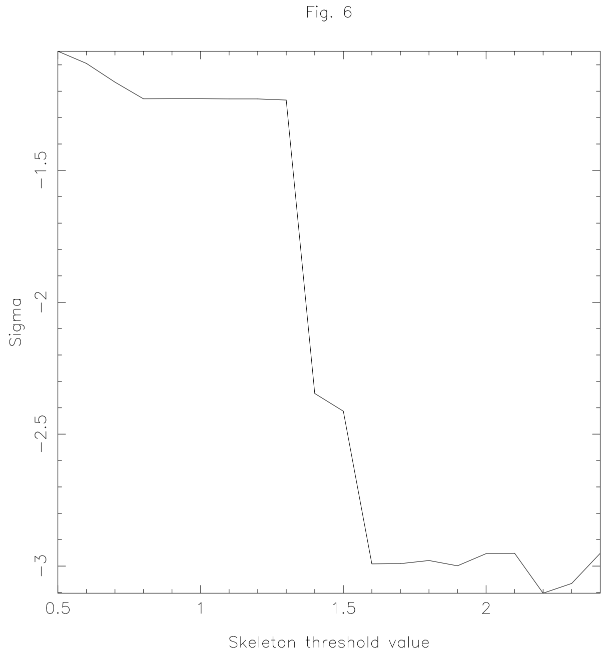

Fig. 6: The standard deviation (in a log scale) of the wavelet coefficients at the smallest scale computed from the reconstructed signals , as a function of T_{sk}

Fig. 6 shows the plot of this standard deviation as a function of T_{sk} (in a semi-log representation). The curve is typically made of plateaus and sharp changes. In each plateau there is no significant change of the reconstructed signal. Each sharp change (when decreasing T_{sk}) corresponds to the adding of new details and eventually some noise. Among a set of discret values of T_{sk}, from 2.5 downto 0.5 sampled by a step of 0.1, we choose the smallest value of T_{sk} for each plateau. This gives us one or several values of T^*_{sk} for which we reconstruct the signal.

Fig. 7 shows the different reconstructed signals as a function of various choices of T_{sk}. One can see how the noise is gradually added as T_{sk} decreases. By a simple look to this series of reconstructed signals (from bottom right to top left), one is tempted to choose as the value of T^*_{sk}, the one before the alteration of the smoothness of the reconstructed signal. Practically, in fig. 7, we would choose $T^*_{sk}(a_i) = 1.6\sigma_{S_{ps}}(a_i)$, which correspond to the lower limit of the plateau in fig. 6.

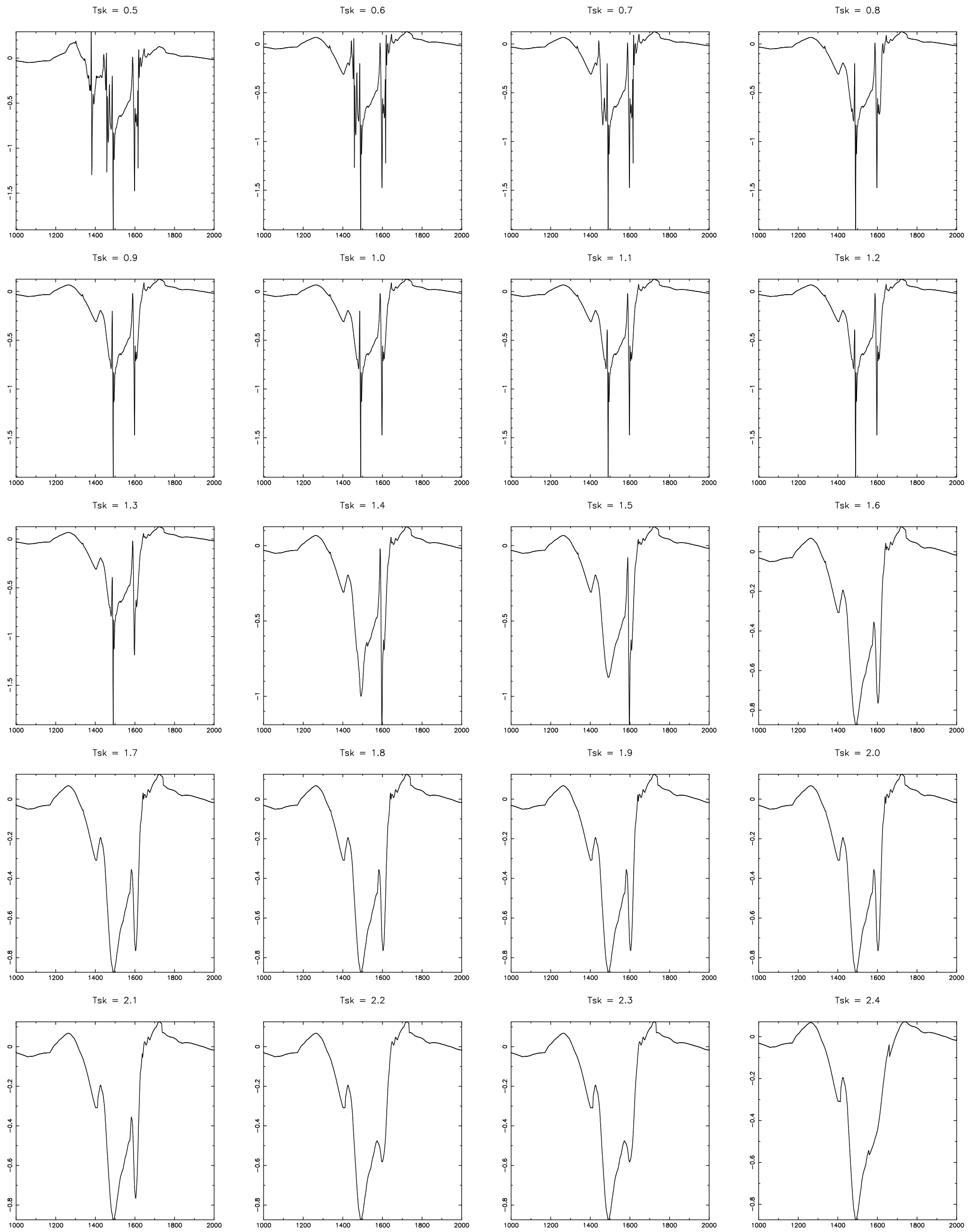

Fig. 7: The series of reconstructed signals (three peaks structures with a noise leading to S/N = 1.2), for a set of T_{sk} from 0.5 to 2.4 with a step of 0.1

Figs. 8 shows the reconstructed signal (full line) superimposed on the simulated noiseless structure (dashed line), for $T^*_{sk}(a_i) = 1.6\sigma_{S_{ps}}(a_i)$. One can appreciate the quality of the reconstruction of this signal with a signal to noise ratio of 1.2 The noise is eliminated and the reconstructed structure has a level of significance of, at least, $1.6\sigma_{S_{ps}}$ (for each scale) versus chance fluctuations which corresponds for a gaussian distribution of the wavelet coefficient to a level of confidence of 94.5 %. However, the core of the structure (the part which is associated to the coefficients selected by $T_{se}(a_i)$) has a level of significance of $5.\sigma_{S_{ps}}$, corresponding to a confidence of 99.99997 %. Thus, the details added with T_{sk} are more significant than other coefficients with amplitudes of the same order of magnitude since they are connected by nearest neighbor relation to this particularly robust core.

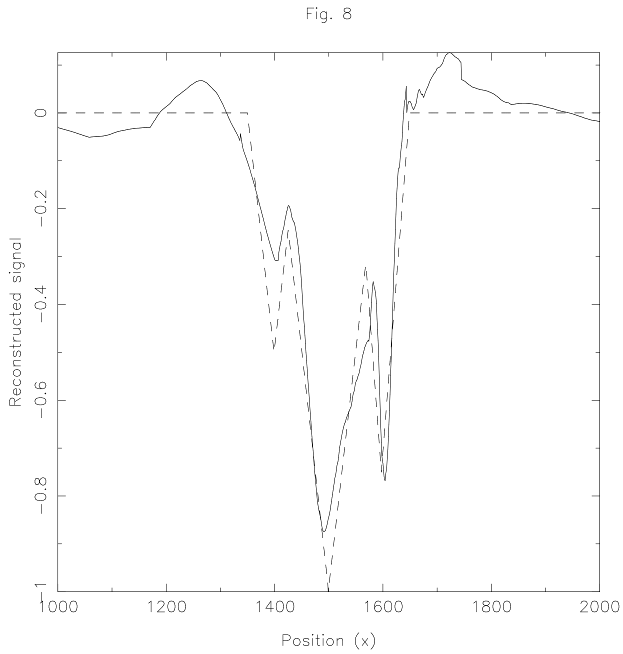

Fig. 8: Full line: the signal reconstructed from the coefficients of Fig. 5c. Dashed line: the initial noiseless signal.

This reconstructed signal is typical of ones that we obtained from several noise simulations. No major discrepancies occurs in the reconstructed signals when different noise realizations are performed. Only the depths of the different peaks varies a little but not significantly. When looking at fig. 8 one can remark that the left peak is less completely reconstructed than the central and right ones. This is due to the presence of the larger and deeper central peak which spoils the detection of this smaller and shallower peak. In fact, there are no coefficients selected by the two thresholding that correspond to that peak. But the presence of the peak modifies the value of the coefficients in the vicinity of the central peak, where we incorporate coefficients to eliminate reconstruction biases. Hence the small branch at scale 7 in Fig. 5b.

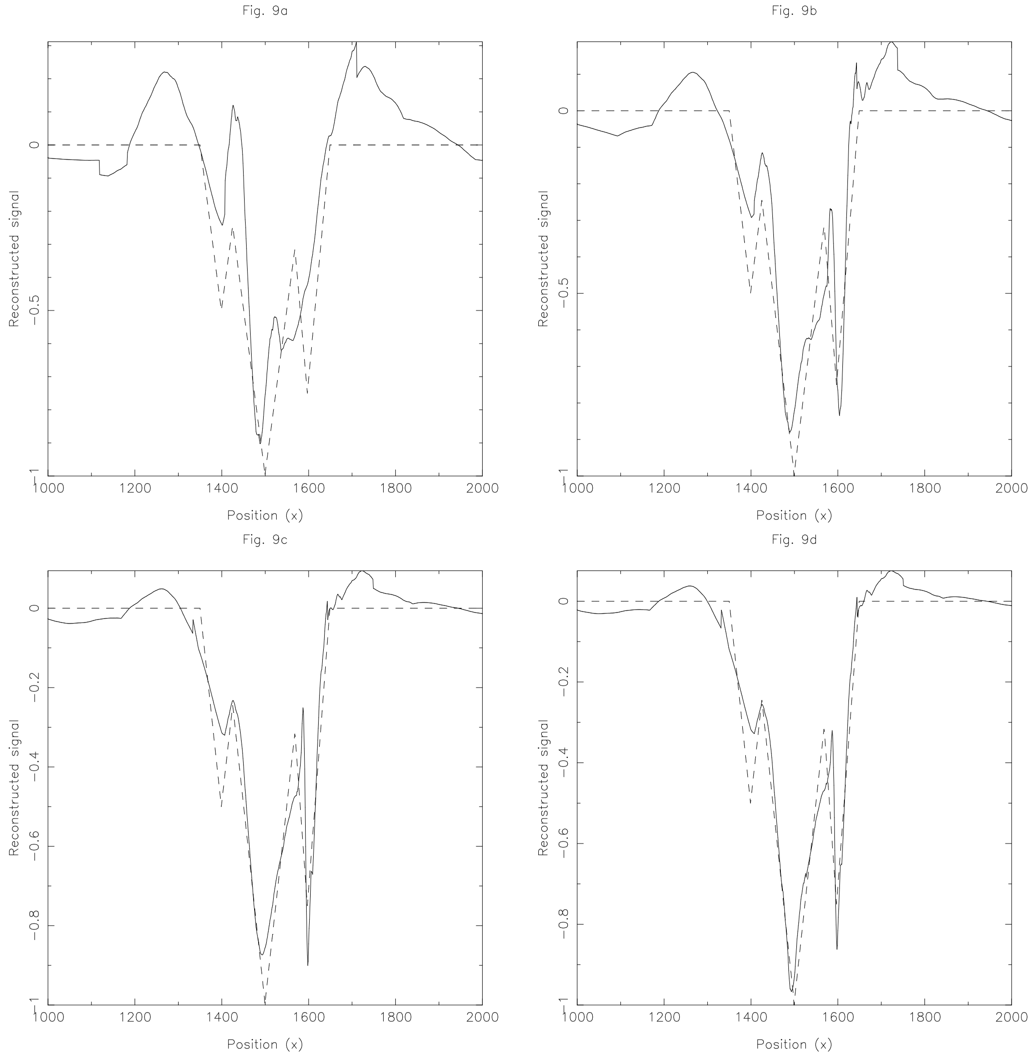

Fig. 9: a) Reconstruction (full line) of a signal similar to that of Fig. 4a, with a signal to noise ratio of 0.4. The second threshold T_{sk} is chosen with the procedure described in section 3.3. The dashed line shows the initial signal before adding the noise. b) Same as Fig. 8a with signal to noise ratio of 0.8. c) Same as Fig. 8a with signal to noise ratio of 1.6. d) Same as Fig. 8a with signal to noise ratio of 2.0.

In addition to the shape of the structure, one can also gain some quantitative information. The depths (or amplitude) of the different peaks and their respective width can be estimated from the reconstructed signal. The estimated widths of the three detected peaks have been found equal to 54, 129 and 38 from left to right which are good estimations of the real values: about 50, 132 and 57 respectively. These widths have been estimated at the base of each peak. The size of the global structure, measured at the base of the left peak, is found to be 249 to be compared to 256 for the real structure. In what concerns the depths we find respectively 0.11, 0.41 and 0.51 to be compared with 0.25, 0.43 and 0.68. The depth of the overall structure, estimated relative to the mean position of the plateau on each side, is 0.88 (true value: 1.0).

In order to have an idea of how the reconstruction process is influenced by the signal to noise ratio, we show in Figs. 9a-d the reconstructed signals for S/N = 0.4, 0.8, 1.6 and 2.0 respectively. Obviously, for very small S/N the algorithm is not able to resolve the internal details of the structure, but it is still able to find it, with the rather good estimate of the size. It appears from these simulations that this method gives satisfying results on signals with signal-to-noise ratio greater than about 0.4.

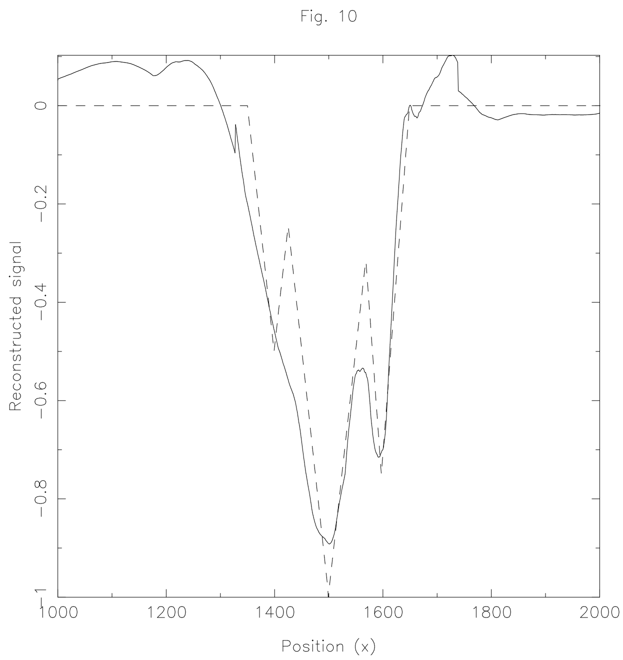

Fig. 10: Reconstruction (full line) of a signal with a signal to noise ratio of 1.2 and a different noise realization from that of Fig. 8. The worst case found in our study.

All the signals we showed up to now have been created with the same realization of the noise, only changing its amplitude. This noise realization was typical of the ensemble. Fig. 10 shows the worst case we have found among different generations of noise and pseudo–random signal for a signal to noise ratio of 1.2. This was the only case nearly as bad, the other ones being closely similar to the reconstruction displayed in fig. 8

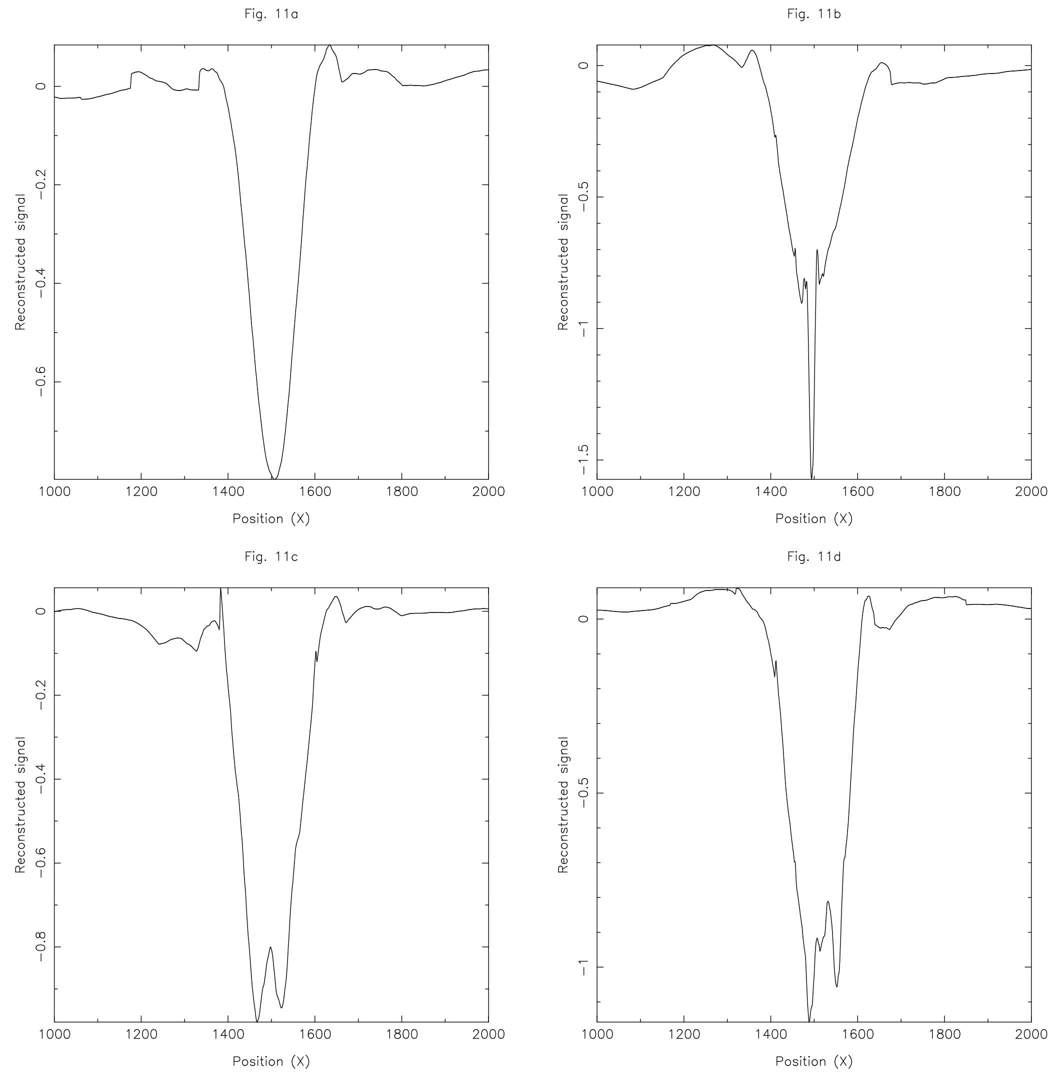

Fig. 11: The four typical kinds of the reconstruction of a single gaussian peak with a signal-to-noise ratio of 1.2. a) smooth mono peak ; b) mono-peak with a very sharp and strong feature ; c) double peak ; d) triple peak.

We have also applied our method to a signal with three Gaussian peaks to test the effect of the shape of the peaks. No significant effect of the structure shape has been found. We have also simulated a single Gaussian peak in order to estimate the percentage and the importance (in a qualitative sense) of false detections of weak features. For this purpose we have generated 100 mono-peak signals with different realizations of the noise, but keeping the same signal-to-noise ratio fixed at 1.2. The structure has been automatically reconstructed following the above described procedure. Four types of reconstructed signals appeared with the following percentages : 1) smooth mono peak (59 %) ; 2) mono-peak with a very sharp and strong feature (12 %) on the side. This kind of feature can unambiguously be interpreted as being due to the presence of a strong localized noise ; 3) a double peak (21 %) 4) a triple peak (8 %). These two later cases are to be qualitatively compared to the simulations of the three peak structures (fig. 8). The four typical kinds of reconstructed peaks are displayed in figs. 11 (a to d respectively for cases 1 to 4)

Summarizing the results of the different reconstructions, we have been able to : (i) recover more than 70 % of mono peaks, (ii) differentiate the false detections of two and three peaks from the real ones (see figs. 11 c-d and 9 a-d), (iii) to detect and reconstruct the three peaks structures even with low signal-to-noise ratio. This have led us to apply the whole procedure, first in the debated, as previously mentioned, Encke gap of the Saturn A ring.

3.4 Data of Voyager in the Encke gap in Saturn's A ring

In the previous section, we have shown the possibilities and also the limitations of the method. Particularly, we have seen that this method tends to eliminate the small peaks rather than adding peaks due to the noise. We will then apply our technique to the PPS Voyager data in order to examine the detailed structure of the ringlet found in the Encke division. Our aim is to give some new and independent information which will validate or invalidate the theory of Spahn (1992).

The PPS data of Voyager 2 have been obtained by counting photons coming from a star of reference and occulted by the different parts of Saturn's rings. Fig. 12 shows the analyzed data in the Encke gap of the Saturn A ring. Since we are counting the number of photons coming through the rings, the smaller the density of ring material, the larger the number plotted. Hence a decrease in the level of the signal (what we have called a depletion) corresponds to an increase of the ring density. The data used here are raw data. This choice has been driven by the wish to avoid any preliminary smoothing as it is done when dealing with the optical depth for which a background must be estimated (see Esposito *et al.* 1987). The overall goal is merely to assess the efficiency of this method.

Figs. 13 a-b display the reconstructed signals with $T_{se}(a_i) = 5\sigma_{S_{ps}}(a_i)$ and $T_{sk}(a_i)/\sigma_{S_{ps}}(a_i) =$

1.3, and 0.8 respectively. The structures have been automatically reconstructed for these two values of T_{sk}, following the criterion we have imposed for the reconstruction. In fig. 13a two peaks are well identified and there is also the trace of a third one (on the right side of the central peak). This later appears when reconstructing from the weaker T_{sk}. Its level of confidence, versus noise fluctuations, is therefore smaller and one can see in fig. 13b how noise is added on the left peak at this level of detection. This means that that this third smallest peak is very close to the level of noise.

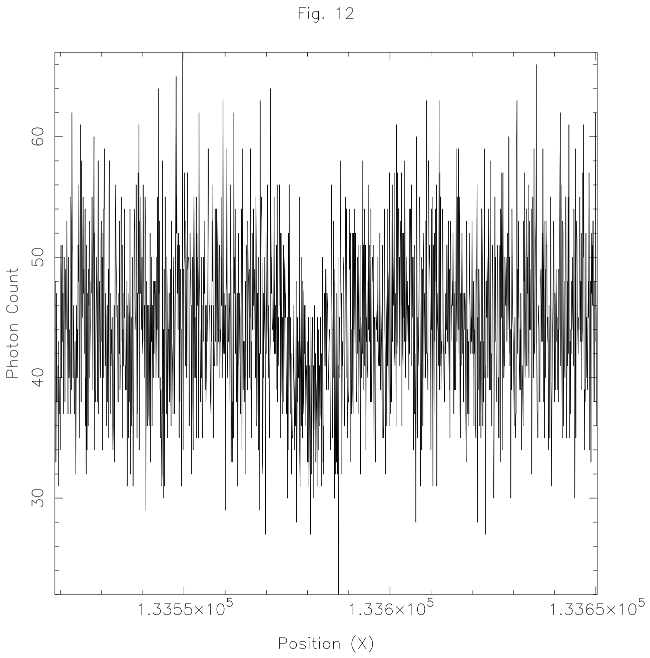

Fig. 12: Voyager 2 PPS data of the Encke gap region in Saturn's rings. The x–axis gives the radial distance from the center of Saturn in kilometers, the y–axis gives the photon counts.

In order to get quantitative information from the reconstructed signal we consider both figures. The global structure is located at 133580.7 km from the center of Saturn and has a typical width of 14.2 km. This value is estimated in fig 13a just above the right peak detected in fig 13b. The left peak is centered at 133576.8 km and has a width of 3.3 km (from fig. 13a). The central one is 8.75 km wide and finally the right one is 3.3 km wide, located at 133586.0 km from the center of Saturn. From the the top of each peak we estimate the depths at 2.2, 2.8, 1.5 units respectively, for the left central and right peaks (keeping in mind that we deal with photon counts, and so, with integers). Finally from the mean position of the plateau on each outer side of the structure the depth of the global feature is measured at 6.5 units.

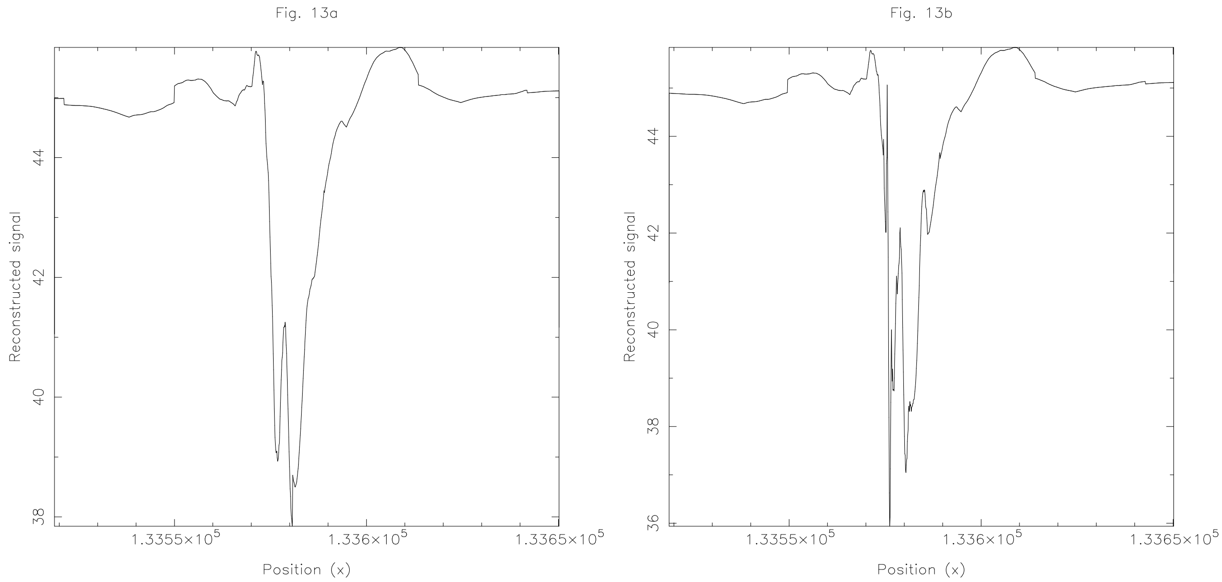

Fig. 13: a) Reconstruction of the signal of Fig. 12 with $T_{sk}(a_i) = 1.3\sigma_{S_{ps}}(a_i)$. b) with $T_{sk}(a_i) = 0.8\sigma_{S_{ps}}(a_i)$.

In order to make some conclusions about the physical parameters of satellite Pan, which is possibly responsible to the ringlet, we plan to apply our method on the results of numerical simulations modelling the interactions between the moonlet and the ring's particles.

In the theory of Spahn, the azimuthally integrated radial density profile was symmetric about the position of the moonlet. But the real ringlet has no reason to be symmetric due to the asymmetry in the position of outer satellites. Moreover, recent numerical simulations show that the radial density profile varies from three to two peaks depending on the azimuth relative to the position of the moonlet.

4 Comparison with other methods

In order to make a rough comparison between our method of structure detection and some already existing techniques, we present in fig. 14 the result of another analysis. This later is a classical one which relies on the use of a low pass filter applied to the Fourier Transform of the signal. The low pass filter is a smooth window with a cut-off frequency from which the higher frequencies are removed from the spectrum of the signal. Theses high frequency components, are mostly noise, and do not contribute to the signal as reconstructed by the inverse Fourier transform. Fig. 14a and 14b display respectively the reconstructed signal for two different widths of the low pass filter.

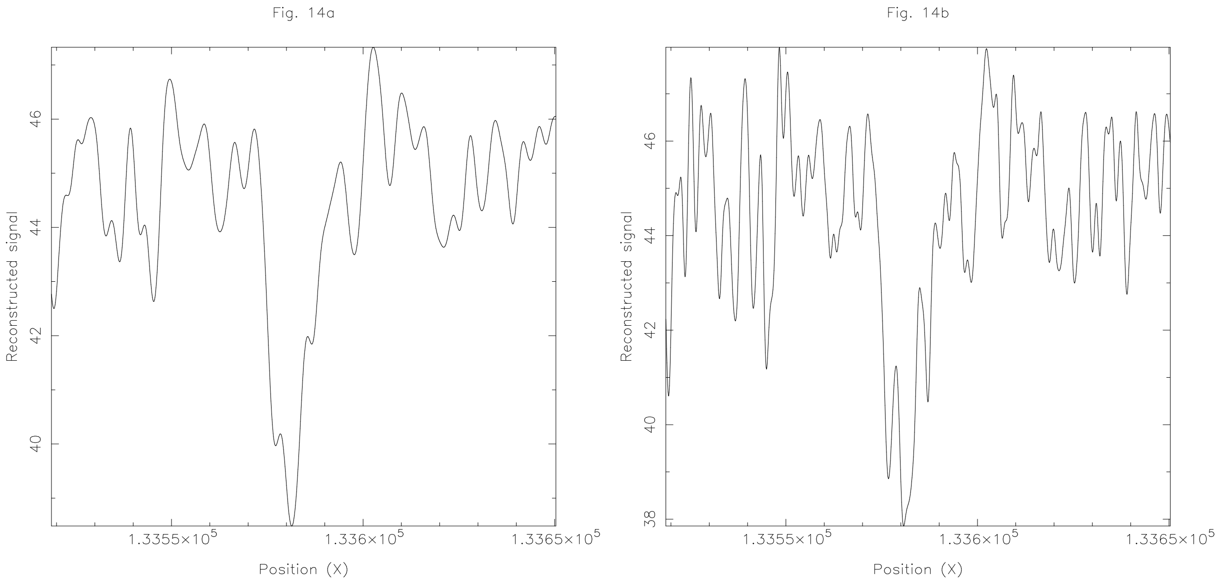

Fig. 14: The same data as in fig.12 analyzed by means of the low pass filter Fourier analysis for 2 different value of the cut-off frequency.

In this method, the noise is globally decreased instead of locally. Hence, it clearly appears that, even if a three peak structure seems to be extracted from the signal the amplitude of the fine features is of the same order of the fluctuations due to the noise. Moreover there is no way to quantify the level of detection of these features and hence to distinguish them quantitatively from the noise.

5 Conclusion

We now have a powerful signal processing tool which is able to detect structures even in a strongly noisy signal and which allows one to quantify the level of significance of the detected structures versus the noise fluctuations. Moreover the quality of the reconstructed signal and the information available through wavelet analyses performed by different wavelets lead to a fairly good estimation of the physical parameters of the detected structures. We have been able to remove the noise from the raw data of the Voyager 2/PPS experiment in the region of the

Encke gap. The Encke gap ringlet exhibits, with a high level of confidence, a two peak profile. According to Spahn *et al.* (1992), this points to a nearly circular orbit of Pan. However, the reconstructed profile shows only qualitative agreement with their model. They obtained very sharp and narrow peaks at the edges, while the right edge of the reconstructed structure is rather smooth (Fig. 13a). On the other hand, taking the size of Pan found by Showalter (1991) of about $20km$ in diameter (icy composition assumed), the satellite should be able to confine a ringlet of width $W > 30km$. But we see only $W \approx 14km$. However, Spahn *et al.* .(1992) showed that the higher the eccentricity of the orbit of the embedded moonlet – here Pan – the smaller the width W of the ringlet (Eq. 8 and Fig. 2 in Spahn *et al.* , 1992). According to their findings the satellite Pan should have an eccentricity of the order of its Hill-scale: $e_{Pan} \approx 10^{-4}$. If we assume that this is correct, then the ringlet should show a three peak structure similar to the artificial signal presented in Fig. 2a. However, there is a hint for the existence of a third peak (albeit of very small amplitude), but with a lower level of confidence.

Recent simulations (Spahn *et al.* , 1993) point at deficiencies of the model of Spahn *et al.* (1992). These new investigations, where the assumption of axisymmetry has been dropped, show that the previous results are correct only if averaged azimuthally, while the actual radial density profile can depend on the azimuthal longitude in the case of eccentric moonlet orbits. So it might happen that one observes a single, or double or also a triple–peaked ringlet profile for the same model-run. Thus the existence of the central and a companion peak cannot be excluded, where the third peak appears even at another azimuthal longitude.

However this first application on the Encke gap ringlet has been performed with raw data (photon count). Since all the theoretical models use either surface mass density or optical depth, some parameters cannot be reached by analyzing raw data. We need to transform these data in optical depth profile in order to obtain the values of these parameters. We are now performing analyses in a systematic way on the Voyager data of Saturn and Uranus rings. The results will be presented in a forthcoming paper.

Appendix A

We describe here the algorithm to add coefficients in order to avoid reconstruction biases. As previously mentioned, a depletion in the signal gives negative coefficients at its location and positive coefficients on each side (see section 2.2 and Fig. 2b). If we don't keep the positive coefficients, the reconstruction will give bumps on each side of the reconstructed depletion. Therefore, we want to keep these coefficients. The algorithm is as follows. For each scale, do:

i find the sets of contiguous coefficients selected by the thresholding, ii on each side of each contiguous set (neighboring in both the scale and location directions), determine a range the size of which is the extent of the wavelet at that scale,

iii in each range, keep the coefficients that are greater [resp. smaller] than the mean for the detection of a depletion [resp. bump],

iv add the coefficients that are smaller [resp. greater] than the mean, but not selected by the thresholding and lie between a set of contiguous selected coefficients and the coefficients added in step (iii) (this avoids discontinuities on the edges of the reconstructed structures).

Acknowledgements

We would like to thank Larry Esposito, Karen Simmons, and Joshua Colwell for providing us with the Voyager-2 PPS-data of planetary rings. We are also very grateful to Jeffrey D. Scargle for his very helpful and meaningful comments. We finally thank Michel Hénon for his suggestions

6 References

[1] Bendjoya, Ph., Slezak, E. & Froeschlé, Cl., 1991. *The wavelet transform: a new tool for asteroid family determination,* Astron. Astrophys., in press, **251** pp. 312–330,

[2] Borderies, N., Goldreich, P. & Tremaine, S., 1989. *The formation of sharp edges in planetary rings by nearby satellites,* Icarus **80** pp. 344–360,

[3] Brophy, T.G. & Rosen, P.A., 1992. *Density waves in Saturn's rings probed by radio and optical occultation: Observational tests of theory,* Icarus **99** pp. 448–467,

[4] Daubechies, I., 1988. *Orthogonal bases of compactly supported wavelets,* Comm. Pure Appl. Math. **41** pp. 909–996,

[5] Esposito, L.W, O'Callahan, M., Simmons, K.E., Hord, C.W., West, R.A., Lane, A.L., Pomphrey, R.B., Coffeen & D.L., Sato, M., 1983*a*. *Voyager photopolarimeter stellar occultation of Saturn's rings,* J. Geophys. Res. **88** pp. 8643–8649,

[6] Esposito, L.W, O'Callahan, M. & West, R.A., 1983*b*. *The structure of Saturn's rings: implications from the Voyager stellar occultations,* Icarus **56** pp. 439–452,

[7] Esposito, L.W., Harris, C.C & Simmons, K.E., 1987. *Features in Saturn's rings,* The Astroph. J. Supp. **63** pp. 749–770,

[8] Grossmann, A., Kronland-Martinet, R. & Morlet, J., 1989. *Reading and understanding continuous wavelet transform,* in *Wavelets, Time-Frequency Methods in Phase Space,* eds. Combes J.M., Grossmann A. and Tchamitchian Ph., Springer-Verlag, pp. 2–20,

[9] Lane, A.L., Hord, C.W., West, R.A., Esposito, L.W., Coffeen, D.L., Sato, M., Simmons, K.E., Pomphrey, R.B. & Morris, R.B., 1982. *Photopolarimetry from Voyager 2: preliminary results on Saturn, Titan and the rings,* Science **215** pp. 537–543,

[10] Mallat, S.G., 1989. *A Theory for Multiresolution Signal Decomposition: The Wavelet Representation,* IEEE Transactions on Pattern Analysis and Machine Intelligence **11** 7, pp. 674–693,

[11] Meyer, Y., 1989. *Orthogonal wavelets,* in *Wavelets, Time-Frequency Methods in Phase Space,* eds. Combes J.M., Grossmann A. and Tchamitchian Ph., Springer-Verlag, pp. 21–37,

[12] Petit, J.M. & Hénon, M., 1988. *A numerical simulation of planetary rings III. Mass segregation, ring confinement, and gap formation,* Astron. Astrophys. **199** pp. 343–356,

[13] Showalter, M., Cuzzi, J.N., Marouf, E.A. & Esposito, L.W., 1986. *Satellite 'wakes' and the orbit of the Encke gap moonlet,* Icarus **66** pp. 297–323,

[14] Showalter, M., 1991. *Visual detection of 1981 S13, Saturn's eighteenth satellite, and its role in the Encke gap,* Nature **351** pp. 709–713,

[15] Spahn, F., Saar, A., Schmidt, S. & Schwarz, U., 1992. *The influence of various moonlets on the optical depth profile in planetary rings,* Icarus **100** pp. 143–153,

[16] Spahn, F. & Scholl, H., 1993. in preparation